Article

Performance Investigation of Single–Piston Free Piston Expander–Linear Generator with Multi–Parameter Based on Simulation Model

Zhuxian Liu [1], Zhong Wu [1,*], Yonghong Xu [1,*], Hongguang Zhang [1], Jian Zhang [2] and Fubin Yang [1]

1   Faculty of Environment and Life, Beijing University of Technology, Pingleyuan No. 100, Beijing 100124, China
2   Mechanical Engineering, University of Wisconsin-Green Bay, 2420 Nicolet Dr., Green Bay, WI 54311, USA
*   Correspondence: wz2009sd@163.com (Z.W.); xyhcomeonljx@126.com (Y.X.)

Abstract: The structural design and operating strategy of a free piston expander–linear generator (FPE–LG) has a major impact on performance. In this paper, the simulation model of single–piston FPE–LG was built and verified by combining the structural parameters of the existing test rig with a set of kinetic and thermodynamic equations. On this basis, the influence of the design and operating parameters of the device on the performance was studied, while keeping other parameters fixed. Then, a sensitivity analysis of power output and operating frequency was carried out. The results show that within a certain range of external load and intake beginning position, increasing the diameter of the intake and exhaust pipes, or reducing the piston rod diameter can improve the power output. Within a certain range of frictional coefficient and intake time, increasing the cylinder diameter and intake pressure, or reducing the piston assembly mass and back electromotive force (EMF) constant can increase the operating frequency. Both the power output and the operating frequency are most sensitive to the cylinder diameter among the design parameters. Among the operating parameters, power output is the most sensitive to intake pressure, and operating frequency is the most sensitive to intake beginning position. The optimization of structural design and operation strategy in expander provides important guiding significance for ORC waste heat recovery system.

Keywords: single–piston free piston expander–linear generator; design and operating parameter; waste heat recovery; sensitivity analysis; simulation model

1. Introduction

In order to achieve the goal of "carbon peaking and carbon neutrality" and create an environment friendly and energy saving society, new energy construction and energy conservation are effective ways that have been focused on and researched extensively. In terms of new energy construction, actively developing and utilizing solar energy [1], wind energy [2], compressed air [3] and other new energy sources to supplement the shortage of conventional energy is widely adopted. Meanwhile, the optimization of energy storage technologies is carried out simultaneously [4,5]. In terms of energy conservation, improving energy conversion efficiency [6] and enhancing waste heat recovery and utilization [7] are the main and most effective ways. Scholars from various countries have improved waste heat recovery devices [8] and non–traditional internal combustion engines (ICEs) [9]. Among them, the organic Rankine cycle (ORC) system has been widely researched in recent years due to its high efficiency [10], compact structure, low cost, and easy use in recovering exhaust heat from ICEs [11]. A basic ORC system mainly consists of four components: expander, condenser, pump, and evaporator. The expander is the main heat-power conversion component in ORC system and plays a vital role.

Researchers around the world have explored different types of expanders in hopes of finding better expanders for ORC systems. Bahadori et al. [12] found that there are problems with turbo expanders in applications where the power output is less than 50 kW,

such as low efficiency and high cost, as well as erosion of blades. The positive displacement expander has potential advantages as an expander for low-power engines such as low-cost, relative high efficiency [13], no large reduction gearbox to change gears, compact structure, and simple controls. Badr et al. [14] compared the three types of expanders i.e., reciprocating piston expander, screw expander, and sliding vane rotary expander, and found that their applicability is determined by many factors such as power capacity, cost, and complexity. Although the reciprocating piston expander is relatively well-developed, it also has certain shortcomings. Compared with reciprocating expanders, the fluid friction loss of the intake and exhaust ports of the sliding vane rotary expander is smaller, the structure is more concise, and the generated noise and vibration are smaller, but the loss and internal leakage and friction dissipation of the intake and exhaust are higher [15]. The screw expander, on the other hand, needs to control the speed due to the high speed. Ziviani et al. [16] experimentally evaluated a newly designed open oil-free scroll expander. The performance of the expander was characterized by a semi-empirical model, and the different loss terms were decomposed to illustrate the main friction losses in bearings, tip seals, and other friction sources. Tarique et al. [17] experimentally studied the performance of ORC systems with a scroll extender. The results show that the scroll expander can effectively use the low-temperature heat source to generate mechanical work or electrical energy. Zhang et al. [18] applied a single–screw expander with a diameter of 155 mm to an ORC system for waste heat recovery from diesel engine exhaust. The results indicate that the maximum power output and total efficiency of single–screw expander are 10.38 kW and 57.88%, respectively. Yang et al. [19] established and tested a combined vehicle system of diesel engine-ORC with screw expander, and found that the power output is higher than that of the diesel engine. Fatigati [20,21] proposed the design concept of a double-inlet vane rotary expander, compared it with the traditional single-inlet expander under the same working conditions, and analyzed its potential to simplify size and increase mechanical efficiency. Oudkerk et al. [22] tested an ORC system with a swash-plate piston expander obtaining its performance map. The effects of pressure ratio, speed, and mechanical efficiency on isentropic efficiency were analyzed, and it is found that the weights of the leakage influencing factors change due to the change in speed. Zheng et al. [23] proposed a kilowatt–sized rolling–piston expander in a low–temperature ORC power generation system and conducted a dynamic test for performance evaluation. The results show that the maximum theoretical efficiency of a CO2 rolling-piston expander is 60%, and the heat and pressure loss in the flow channel is large. Li et al. [24] proposed a double-piston free-piston expander-linear generator with high temperature and high-pressure gas as working fluid to generate electricity and found that it has the potential for small ORC applications due to its simple and compact structure and no crank connecting rod mechanism. The ORC system used in ICEs waste heat recovery is of small scale, which has a power output generally less than 15 kW. Therefore, investigating and designing an applicable small and efficient expander is of great significance.

Since the first development of free piston expander (FPE) at the Technical University of Dresden, the device has received great attention from academia and industry [25]. FPE has the advantages of compact structure, small friction loss, good sealing, and high efficiency, thus solving the problems of sealing and lubrication existing in most low–power expanders, and it satisfies the requirements for expanders in ORC applications. Zhang et al. [26] designed a double acting FPE and verified its operating process. The device improved the performance of transcritical CO2 cycle system, reaching an isentropic efficiency of 62%. The optimal operating frequency is found to be from 10 to 17 Hz. However, there are few investigations of the structural design and operating strategy of the system involved in their study. Weiss et al. [27] designed a millimeter–scale FPE and discussed the influence of piston mass on its performance. The results show that decreasing the piston mass can reduce stroke and increase operating frequency and power output. Then they explored the effect of design and operating parameters such as piston mass, external load, and heat input on the performance of FPE [28]. The results show that increasing the heat inputs to FPE can

reduce operating frequency and increase power output. Moreover, they improved system performance by optimizing variables including piston mass, FPE size, input pressure, and lubrication [29]. The results indicate that FPE efficiency, operating frequency, and power output are sensitive to factors such as input pressure, piston mass, and external load. [30] However, there are few horizontal comparisons of these parameters involved in this paper, and the impact of these variables on performance remains to be studied. Li et al. [24] proposed an FPE–LG integrated unit with a plate-type linear generator (LG) and a cam plate intake and exhaust mechanism. By means of experiments [31] and simulations, the operating and output characteristics of FPE–LG were studied. However, due to the fixed structure of cam plate, the intake and exhaust timing of the device has certain limitations. Hou et al. [32] improved the intake and exhaust system by adopting a servo motor control system and conducted further analysis of its performance. The results indicate that the selection and design of LG have a significant influence on FPE–LG performance. Intake pressure and external load have a great influence on actual stroke and velocity [33]. It is feasible to improve the conversion efficiency of the FPE–LG by increasing the intake pressure [34]. Aziz et al. [35] studied a dual–piston FPE–LG by changing various intake pressures and generator stator cores. The effect of these variables on the root mean square power output, as well as the system stability and conversion efficiency were explored. The results show that when the valve opening duration increases, the indicated efficiency and power-to-electricity conversion efficiency increase. Also, different generator stator cores have an influence on operating frequency and power output [36]. Wang et al. [37] built a test rig of a dual–piston FPE–LG and investigated the output voltage and energy conversion efficiency of device. The results show that the energy conversion efficiency increases with higher intake pressure, and can reach up to 55% with an intake pressure of 3.75 bar. Xu et al. [38] established and validated an integrated model of a compressed air-driven two–stroke free piston engine system using MATLAB/simulink. The power output and efficiency of permanent magnet linear generators under different intake pressures and external loads were obtained. The results reveal variation laws of piston displacement, velocity, and frequency with the intake pressure and piston assembly mass. However, there are few design parameters involved in this paper, and the effect of design parameters on the system performance remains to be studied. Peng et al. [39] established a test rig of FPE–LG system coupled with the drive motor, and investigated the operating characteristics of FPE–LG under different torques and expansion times. Li et al. [40] presented a single–piston FPE–LG prototype for a small–scale ORC system, and proposed and verified two control strategies. Wu et al. [41] investigated the performance of the single–piston FPE–LG using position–time control method. The results show that the bias displacement and indicated work increased with increase of intake time or intake pressure. Also, it was found that the energy loss due to air resistance accounts for the highest proportion, up to more than 50% [42]

The above literature review shows that as a new type of power machine, FPE–LG has great potential in the field of power and waste heat recovery, which has stimulated the research of scholars all around the world. However, the research on FPE–LG is still in the exploratory stage. Due to the limitations of the test rig, the mechanism of some design and operating parameters on performance of FPE–LG have not been studied in depth. Therefore, it is necessary to establish a more effective simulation model to conduct in–depth research on the influence mechanism of main design and operating parameters on the FPE-LG performance. In this paper, based on existing single–piston FPE–LG test rig, a simulation model is built and coupled with dynamic and thermodynamic equations. The influence of design parameters (piston assembly mass, back EMF constant, frictional coefficient, piston rod diameter, cylinder diameter, and diameter of intake and exhaust pipes) and operating parameters (intake beginning point, intake time, intake pressure, and external load) on the FPE-LG performance were studied in depth. The research results have important guiding significance for the efficiency improvement of the expander in ORC system, and can provide directions for the optimization of structure design and operation

strategy. It has great potential for ORC waste heat recovery system to improve energy recovery efficiency with an optimized FPE-LG.

2. Methodology

2.1. Test Rig Description

The FPE–LG test rig is shown in Figure 1. The test rig mainly includes FPE, LG, signal acquisition and control system (SACS), flow meter, regulating valve, solenoid valve, various sensors, and external load. The working fluid is compressed air. There are experiment data collected on SACS including the velocity and position of the piston assembly, pressure in-cylinder, voltage, and current of output. The main parameters of the test rig are shown in Table 1. The schematic of FPE–LG is shown in Figure 2.
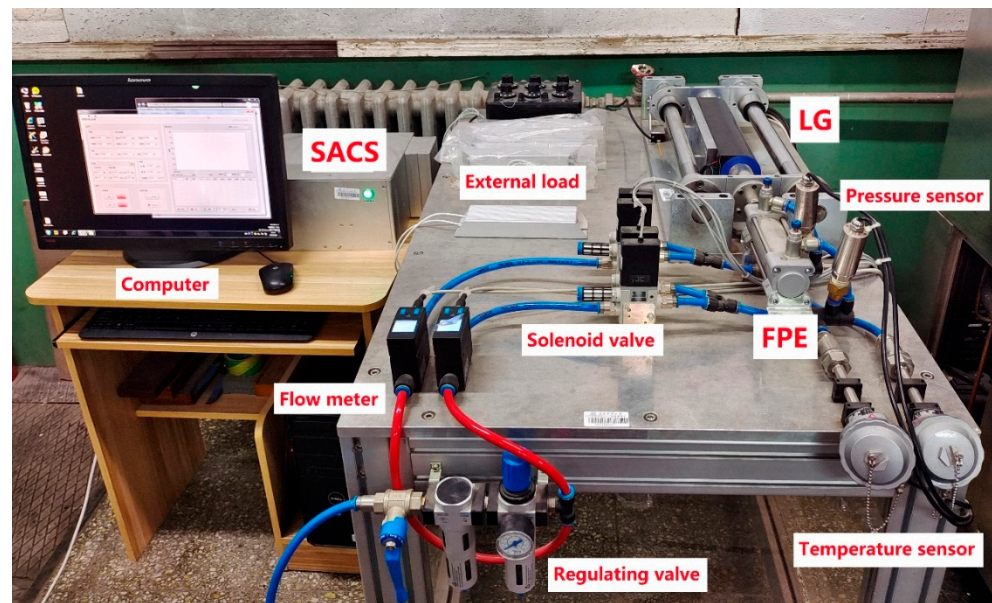

Figure 1. Single–piston FPE–LG test rig.

Table 1. Main parameters of FPE–LG.

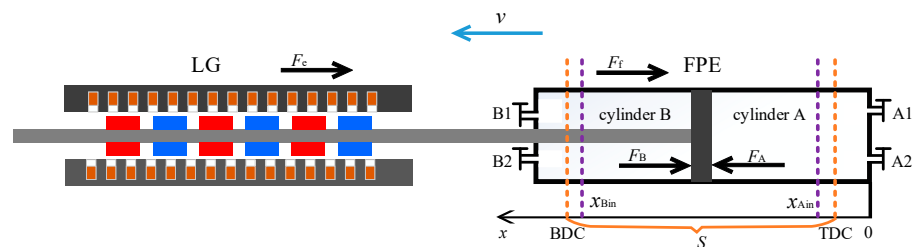| Parameters	Value	Unit
Cylinder diameter	40	mm
Working pressure	1–10	bar
Maximum stroke	70	mm
Piston rod diameter	16	mm

Figure 2. Schematic of the single–piston FPE–LG.

When the piston moves to the position where the volume of cylinder A is minimum, the position is set as 0 point. When the piston moves to the position where intake regulating valves in cylinder A/B are opened, this position is considered as the intake beginning position A/B, as shown in xAin/xBin in Figure 2. Since it takes time to increase the pressure in the cylinder, there is a time lag between TDC/BDC and xAin/xBin. The displacement from TDC to BDC is the stroke S. In this paper, we used the position-time control method on this test rig, which needs to set the intake time tAin/tBin, and intake beginning position xAin/xBin in advance in SACS to control the solenoid valves to implement the intake and exhaust process. Among them, solenoid valves 1 is the intake port and solenoid valves 2 is the exhaust port. The schematic of position-time control method is shown in Figure 3, and more details of the method can be found in our previous paper [42].
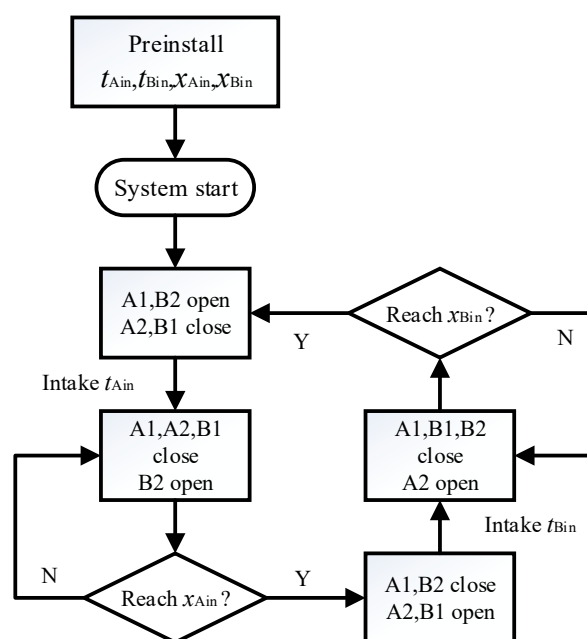

Figure 3. Schematic of position-time control method.

2.2. Submodel of FPE–LG

In order to find out the performance characteristics of FPE–LG, the FPE-LG sub-model was built. To simplify the formulas used in this model, the following assumptions need to be made [38]:

(1)   The working fluid behaves like an ideal gas;
(2)   The state of working fluid in the same cylinder is uniform, the temperature field and pressure field of fluid are uniformly distributed, and the intake air flowing into the cylinder is instantly and completely mixed with the residual air during intake stage;
(3)   The pressure drop in the intake and exhaust pipes is neglected;
(4)   There is no leakage between the cylinders on both sides of piston, and no leakage at the connection of each component;
(5)   The air in cylinder undergoes a polytropic process during the expansion stage.

When FPE–LG is operating, piston assembly is the main research object, of which the movement is determined by the net force acting on it. As shown in Figure 2, during the operation the piston assembly is affected by gas forces F_A and F_B that exerted by air on the left and right sides of piston, frictional force F_f, and electromagnetic force F_e.

According to the above mentioned assumptions, the single–piston FPE–LG system can be simplified as an integrated system, which is subject to the gas force on both sides of

piston, the electromagnetic resistance, and the frictional resistance. According to Newton's second law, the dynamic formula of piston assembly in single–piston FPE–LG is established:

$$\vec{F}_A + \vec{F}_B + \vec{F}_f + \vec{F}_e = m\frac{d^2s}{dt^2} \tag{1}$$

where F_A is the gas force exerted on the piston by the air in cylinder A, F_B is the gas force exerted on the piston by air in cylinder B, F_e is the electromagnetic resistance, F_f is the frictional resistance, m is the piston assembly mass, s is the displacement of piston, and $\frac{d^2s}{dt^2}$ is the acceleration of piston assembly.

This model is built mainly to analyze the forces on the piston. Therefore, it is necessary to calculate the variation of intake and exhaust flow, in–cylinder pressure, induced electromotive force, and frictional resistance with time.

2.2.1. Cylinder Process Model

According to the assumption (3), the flow areas of air vary with time, and the air flow process can be approximately treated as a one–dimensional isentropic adiabatic process. The exhaust stage can be considered as the reverse of intake stage [38].

When $\frac{p_e}{p} < (\frac{2}{k+1})^{\frac{k}{k-1}}$, the cylinder is in a supercritical state, and the change rate of the intake or exhaust flow is:

$$\frac{dm}{dt} = \mu_e \cdot A\frac{p}{\sqrt{RT}} \cdot (\frac{2}{k+1})^{\frac{1}{k-1}} \cdot \sqrt{\frac{2k}{k+1}} \tag{2}$$

When $\frac{p_e}{p} \geq (\frac{2}{k+1})^{\frac{k}{k-1}}$, the cylinder is in a subcritical state, and the change rate of intake or exhaust flow is:

$$\frac{dm}{dt} = \mu_e \cdot A\frac{p}{\sqrt{RT}} \cdot \sqrt{\frac{2k}{k-1} \cdot [(\frac{p_e}{p})^{\frac{2}{k}} - (\frac{p_e}{p})^{\frac{k+1}{k}}]} \tag{3}$$

where p_e is the intake or exhaust pressure, k is the adiabatic coefficient, μ_e is the flow coefficient, A is the contact area between air and piston in the cylinder, R is the ideal gas constant, and T is the temperature of working fluid.

According to the assumption (4), in the cylinder of single–piston FPE–LG, there is no mass exchange between the working fluid and the outside during the expansion stage, thus the air mass remains constant at this stage.

The pressure in the expansion stage is calculated by the following formula [43]:

$$p = p'\left(\frac{V'}{V}\right)^k \tag{4}$$

where p' is the in–cylinder pressure in the previous step, and V' is volume of the cylinder in the previous step.

2.2.2. Generator Model

According to Kirchhoff's voltage law, the induced electromotive force generated by the reciprocating motion of motor mover cutting magnetic field lines can be expressed as [44]:

$$E(t) = (R_S + R_e)I(t) + L\frac{dI(t)}{dt} + C\int Idt = -K_v \cdot v \tag{5}$$

where R_S is the resistance in stator coil of generator, R_e is the external load, K_v is the back EMF constant which is determined by the design parameters of generator, and v is the velocity of piston assembly.

When the linear generator is in working state, since the values of inductance *L* and capacitance *C* are very small, the influence of these two parameters on the induced current is ignored in the established model. Combining the above formula, it can be obtained that the induced current generation due to cutting magnetic field lines by the reciprocating motion of motor mover is:

$$I(t) = -\frac{K_v}{(R_S + R_e)}v \tag{6}$$

Based on the electromagnetic resistance calculation formula mentioned in our previous paper [42], the corresponding electromagnetic resistance can be obtained.

2.2.3. Generator Model

The frictional resistance of single–piston FPE–LG consists mainly of the resistance between the piston and cylinder wall, and the resistance between the connecting plate and guide rail. Among them, the frictional resistance between the piston and cylinder wall is impacted by many factors, such as lubrication, working pressure, back pressure, seal design, and so on. In the test rig in this study, there is no relevant instrument for frictional resistance measurement. The frictional resistance was obtained indirectly through calculation. From the analysis [45], it can be seen that the change curve of frictional resistance is consistent with the velocity curve. Besides, other relevant research also concluded that frictional resistance is related to velocity. Therefore, the frictional resistance formula used in the simulation is:

$$F_f = -C_f v \tag{7}$$

where C_f is frictional coefficient.

2.3. Integrated Model

According to above analysis, the FPE-LG simulation model is built in MATLAB/simulink and consists of motion main module, volume calculation module, mass flow calculation module, state transition control module, gas force calculation module, frictional resistance calculation module, electromagnetic resistance calculation module, current calculation module, and voltage calculation module, as shown in Figure 4. And the main parameters of the FPE-LG model are listed in Table 2. To prevent the displacement of piston assembly from exceeding the length of the cylinder during the simulation process, a saturation module was used to control the displacement.
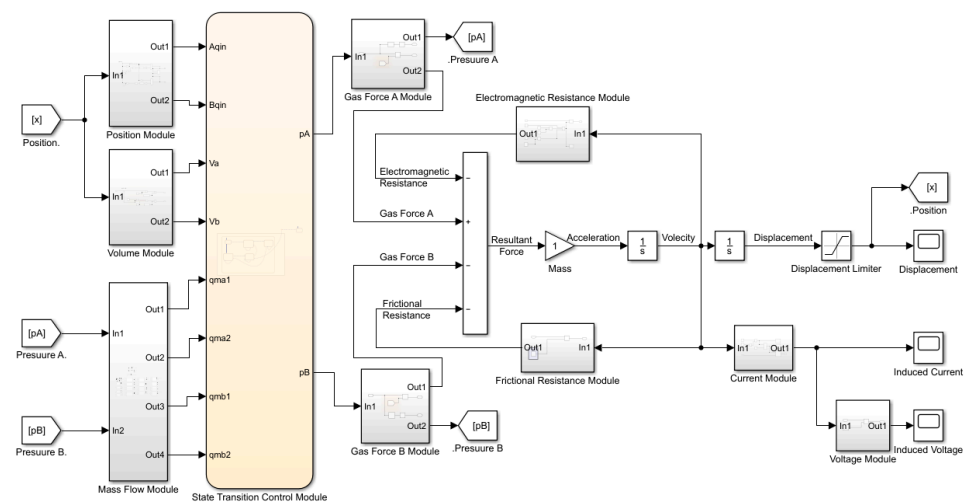

Figure 4. The model of single–piston FPE–LG.

Table 2. Main parameters of FPE–LG model.

Parameters	Value	Unit
Thrust coefficient	75	$N \cdot A^{-1}$
Internal resistance	36.6	Ω
Mass of motor mover	3.7	kg
Cylinder diameter	40	mm
Piston rod diameter	16	mm
Diameter of intake or exhaust pipes	11	mm
Gas adiabatic index	1.4	—
Gas emission factor	0.8	—

2.4. Validity Verification of Model

The MATLAB/simulink simulation model needs to be verified in order to ensure its validity and accuracy. In this section, the output characteristics calculated by the model are compared with those obtained by test rig results under the same operating conditions. The operating condition is shown in Table 3.

Table 3. The operating condition of experimental tests.

Condition	Intake Beginning Position (mm)	Intake Pressure (bar)	Intake Time (ms)
1	21–45	4	30
2	21–45	4	35
3	21–49	4	30
4	21–49	4	35
5	25–45	4	30
6	25–45	4	35
7	21–45	5	30
8	21–45	5	35
9	21–49	5	30
10	21–49	5	35
11	25–45	5	30
12	25–45	5	35

2.4.1. Operating Characteristics

The validation of operating frequency, velocity v_1 (the velocity of piston assembly from top dead center, TDC, to bottom dead center, BDC), velocity v_2 (the velocity of piston assembly from BDC to TDC), and stroke under the selected operating conditions are shown in Tables 4–7, respectively. The validation includes simulation results, experimental test results, and the absolute and relative errors between them. It can be seen that the relative errors of the parameters discussed under all operating points are within ±10%.

Table 4. The validation of operating frequency.

Condition	Simulation Value (Hz)	Test Value (Hz)	Absolute Errors (Hz)	Relative Errors (%)
1	5.57	5.56	0.01	0.18
2	5.62	5.65	−0.03	−0.60
3	5.13	5.13	0.00	0.04
4	5.18	5.26	−0.08	−1.60
5	5.90	5.92	−0.02	−0.29
6	5.87	5.99	−0.12	−1.99
7	6.31	6.02	0.29	4.83
8	6.24	6.10	0.14	2.23
9	5.88	5.65	0.23	4.07
10	5.83	5.68	0.15	2.62
11	6.49	6.25	0.24	3.90
12	6.37	6.33	0.04	0.63

Table 5. The validation of v_1.

Condition	Simulation Value (m/s)	Test Value (m/s)	Absolute Errors (m/s)	Relative Errors (%)
1	0.5967	0.5634	0.0333	5.91
2	0.6423	0.6150	0.0273	4.44
3	0.5760	0.5556	0.0204	3.67
4	0.6217	0.6077	0.0140	2.30
5	0.5885	0.5707	0.0178	3.12
6	0.6293	0.6162	0.0131	2.13
7	0.7053	0.7157	−0.0104	−1.45
8	0.7435	0.7727	−0.0292	−3.78
9	0.6890	0.6973	−0.0083	−1.19
10	0.7352	0.7666	−0.0314	−4.10
11	0.6904	0.7245	−0.0341	−4.71
12	0.7951	0.7805	0.0146	1.87

Table 6. The validation of v_2.

Condition	Simulation Value (m/s)	Test Value (m/s)	Absolute Errors (m/s)	Relative Errors (%)
1	0.5382	0.5444	−0.0062	−1.14
2	0.5582	0.5769	−0.0187	−3.24
3	0.5411	0.5308	0.0103	1.94
4	0.5625	0.5702	−0.0077	−1.35
5	0.5313	0.5313	0.0000	0.00
6	0.5368	0.5748	−0.0380	−6.61
7	0.6395	0.6864	−0.0469	−6.83
8	0.6777	0.7276	−0.0499	−6.86
9	0.6452	0.6683	−0.0231	−3.46
10	0.6577	0.7065	−0.0488	−6.91
11	0.6214	0.6707	−0.0493	−7.35
12	0.6657	0.7137	−0.0480	−6.73

Table 7. The validation of stroke.

Condition	Simulation Value (mm)	Test Value (mm)	Absolute Errors (mm)	Relative Errors (%)
1	34.59	35.43	−0.84	−2.37
2	35.59	37.18	−1.59	−4.28
3	36.08	33.12	2.96	8.94
4	37.03	34.97	2.06	5.89
5	35.60	37.74	−2.14	−5.67
6	37.13	39.58	−2.45	−6.19
7	38.43	42.52	−4.09	−9.62
8	40.54	44.65	−4.11	−9.20
9	37.69	40.01	−2.32	−5.80
10	38.12	42.19	−4.07	−9.65
11	40.75	44.68	−3.93	−8.80
12	42.98	46.65	−3.67	−7.87

2.4.2. Output Characteristics

The validation of power output and single–cycle electric energy output under the selected operating conditions is shown in Tables 8 and 9, respectively. It can be seen that the relative errors of the parameters discussed under all operating conditions are within ±10%.

Table 8. The validation of power output.

Condition	Simulation Value (W)	Test Value (W)	Absolute Errors (W)	Relative Errors (%)
1	16.31	15.36	0.95	6.18
2	17.8	17.71	0.09	0.51
3	15.11	14.60	0.51	3.49
4	16.55	17.09	−0.54	−3.16
5	16.04	15.35	0.69	4.50
6	16.84	17.79	−0.95	−5.34
7	28.03	26.23	1.80	6.86
8	30.08	29.89	0.19	0.64
9	26.99	25.23	1.76	6.98
10	28.04	28.25	−0.21	−0.74
11	27.02	25.20	1.82	7.22
12	27.98	28.87	−0.89	−3.08

Table 9. The validation of electric energy output.

Condition	Simulation Value (J)	Test Value (J)	Absolute Errors (J)	Relative Errors (%)
1	2.93	2.76	0.17	6.09
2	3.17	3.14	0.03	0.94
3	2.94	2.85	0.09	3.31
4	3.20	3.25	−0.05	−1.62
5	2.72	2.59	0.13	4.91
6	2.87	2.97	−0.10	−3.42
7	4.43	4.35	0.08	1.94
8	4.82	4.90	−0.08	−1.56
9	4.59	4.47	0.12	2.69
10	4.81	4.97	−0.16	−3.21
11	4.10	4.03	0.07	1.68
12	4.39	4.56	−0.17	−3.67

In this study, the relative errors between the simulation results and the experimental test results are within ±10%, therefore, the single–piston FPE–LG model is considered to be effective. It has high reliability, and can be used to analyze and predict the operating and output characteristics of FPE-LG under different operating conditions.

3. Result and Discussion

In order to eliminate the dimensional influence between data, data standardization processing is required to solve the comparability between data. After the original data is standardized, each set of data is in the same order of magnitude, thus being suitable for comprehensive comparative evaluation. The standardization method used in this paper is normalization. After the normalizing process, each performance parameter is scaled between 0 and 1 and retains the distribution of the original data.

The calculation formula of normalization is:

$$y_i = \frac{x_i}{x_{\max}} \tag{8}$$

where x_i is the value of performance parameters under operating condition i, $x_{\max}$ is the maximum value of performance parameters obtained, and y_i is the normalized value of performance parameters under operating condition i.

In order to facilitate study, these parameters were analyzed under the operating conditions of p_{in} = 4 bar, t_{in} = 35 ms, and intake beginning position is 21–49 mm.

3.1. Design Parameters

3.1.1. Piston Assembly Mass

Figure 5 shows the variation of normalized value of performance parameters with piston assembly mass m. Figure 5a shows the variation curves of operating frequency f, stroke S, BDC and TDC with piston assembly mass, while Figure 5b shows the variation curves of maximum velocity v_{1max}, maximum velocity v_{2max}, mean velocity $\bar{v}$ (the mean velocity of piston assembly in one period) and power output p with piston assembly mass. With the increase of piston assembly mass, $\bar{v}$ and power output first increase and then decrease, and the trend of two curves is the same, which means power output is related to $\bar{v}$. With the increase of piston assembly mass, TDC decreases while BDC and stroke S increase, that is, TDC moves to 0 point, BDC moves away from 0 point, and stroke increases gradually. Besides, Figure 5 shows that operating frequency, v_{1max}, and v_{2max} decrease, and the decrease of v_{1max} is smaller than that of v_{2max}. Comparing the operating frequency with $\bar{v}$, v_{1max}, and v_{2max} in Figure 5, it can be found that operating frequency is closer to v_{2max}, which means that the operating frequency is more affected by v_2. The change range of TDC with piston assembly mass is smaller than that of BDC, which means that the center of stroke gradually moves away from 0 point. When the piston assembly mass increases, the inertia of the piston assembly will increase, making the stroke increase. The increased stroke will increase the energy consumption of air resistance in the cylinder, decrease v_{1max} and v_{2max}, and increase the period. Due to the interaction of stroke and operating frequency, $\bar{v}$ increases first and then decreases, which leads the power output to increase first and then decrease. The maximum value can reach up to 17.59 W.
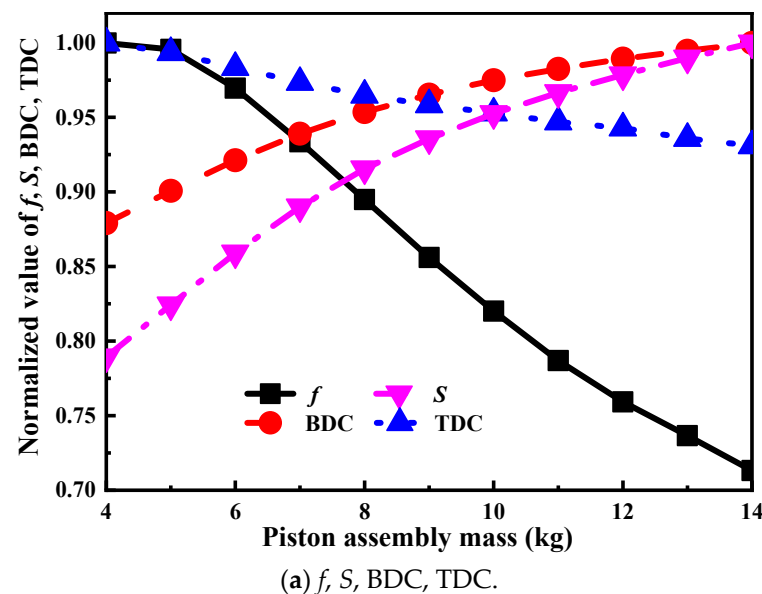

(**a**) f, S, BDC, TDC.

Figure 5. *Cont.*

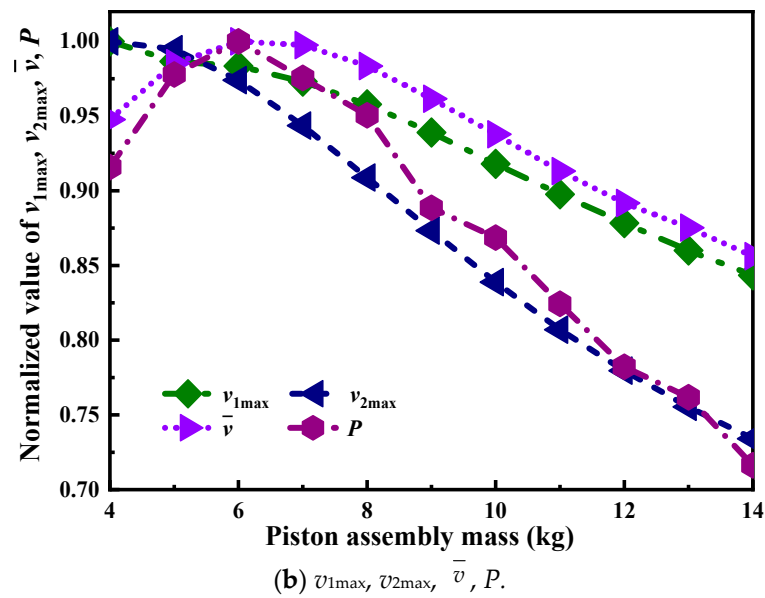**(b)** v_{1max}, v_{2max}, $\bar{v}$, P.

Figure 5. Variation of performance parameters with piston assembly mass.

3.1.2. Back EMF Constant

When the external load and internal resistance of the generator are constant, the electromagnetic coefficient is proportional to back EMF constant [46], so the influence of the electromagnetic coefficient on performance parameters can be regarded as the effect of back EMF constant on the performance parameters. Figure 6 shows the variation of the normalized value of the performance parameters with back EMF constant. It can be seen that all performance parameters except power output decrease with the increase of back EMF constant. The increased back EMF constant could increase electromagnetic resistance generated by LG and reduce the acceleration of piston assembly, thereby reducing the velocity of the piston assembly and shortening the stroke and operating frequency. Finally, the influence of back EMF constant is greater than that of velocity, making the power output increase. The maximum value can reach up to 23.78 W.

(a) *f*, *S*, BDC, TDC.

Figure 6. *Cont.*

(**b**) v_{1max}, v_{2max}, $\bar{v}$, P.
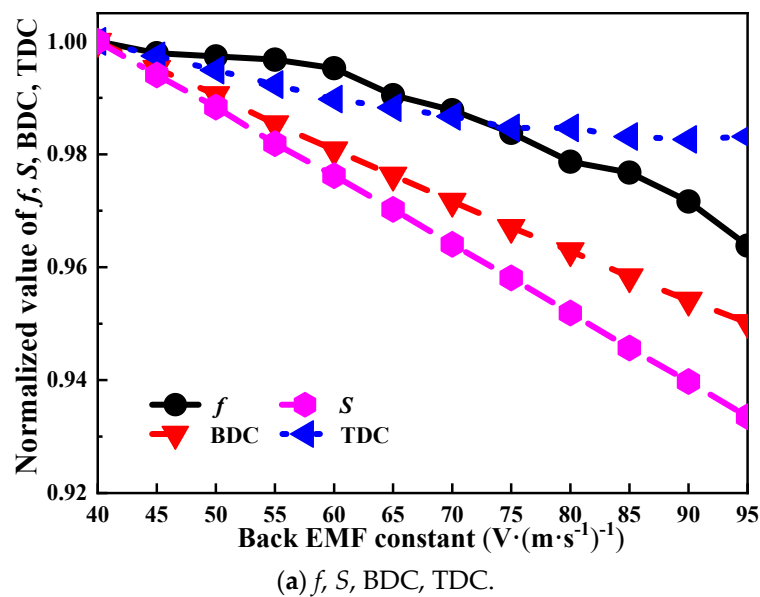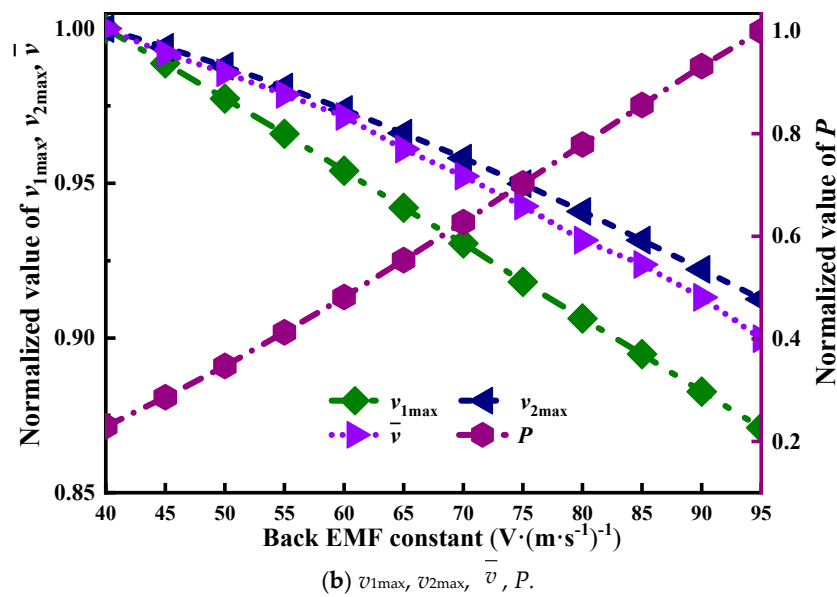
Figure 6. Variation of performance parameters with back EMF constant.

3.1.3. Frictional Coefficient

For FPE, reducing frictional resistance is one of main problems to be solved presently [45]. In real test processes, lubricating oil is commonly used to reduce frictional resistance. In the simulation model, the effect of the frictional coefficient on the performance parameters is discussed. Figure 7 shows the variation of normalized value of the performance parameters with the frictional coefficient. The operating frequency first increases and then decreases, and all other performance parameters decrease with the increase of frictional coefficient. The increased frictional coefficient could increase the frictional resistance and reduce the acceleration of the piston assembly, thereby reducing the velocity of the piston assembly and shortening the stroke and operating frequency. Thus, the velocity of motor mover cutting the magnetic field line is reduced, which leads the induced current and voltage, as well as the power output to reduce. The maximum value of power output can reach up to 20.73 W.
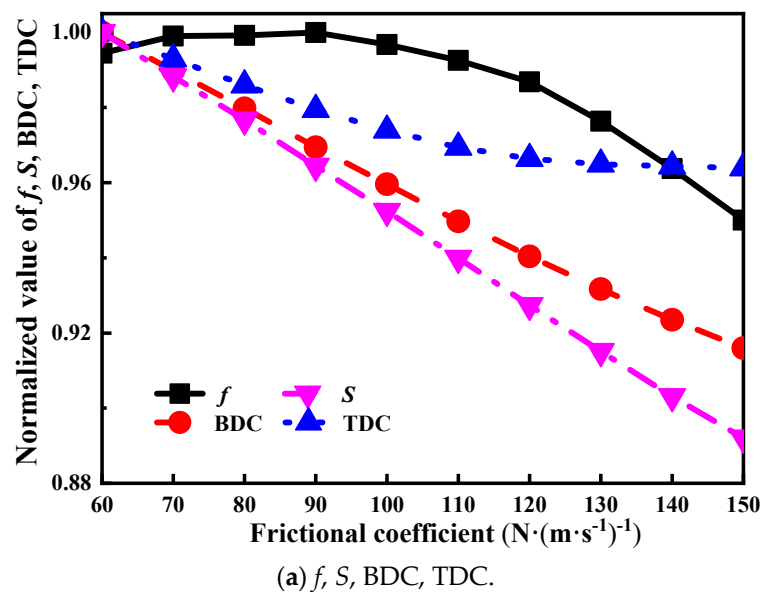

(**a**) f, S, BDC, TDC.

Figure 7. *Cont.*

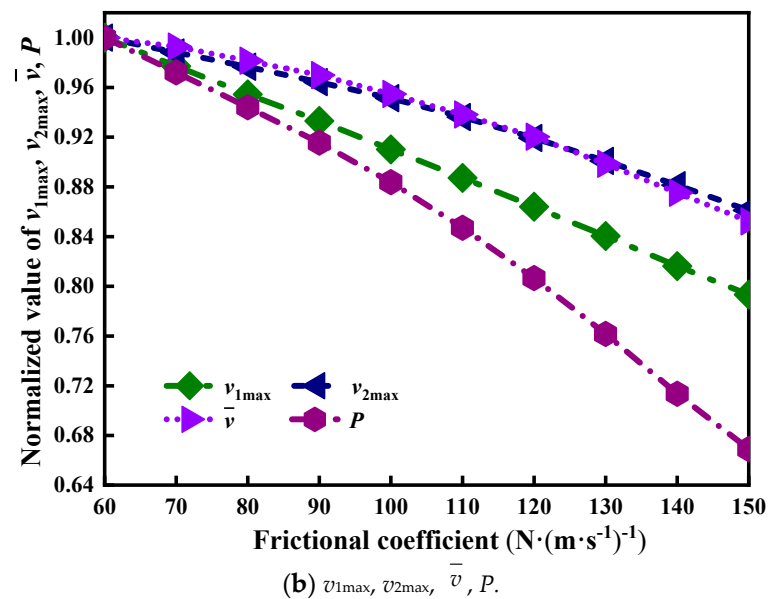**(b)** v_{1max}, v_{2max}, $\overline{v}$, P.

Figure 7. Variation of performance parameters with frictional coefficient.

3.1.4. Piston Rod Diameter

Figure 8 shows the variation of normalized value of performance parameters with piston rod diameter. The change in the piston rod diameter has almost no effect on the stroke. When the piston rod diameter increases, TDC and BDC increase, that is, TDC and BDC are far away from 0 point. With the increase of the piston rod diameter, the proportion of change in TDC is greater than that in BDC, which results in a tiny change of the stroke. As the piston rod diameter increases, v_{1max}, v_{2max}, and $\overline{v}$ tend to decrease. Considering the stroke has almost no change, the decrease of $\overline{v}$ causes the operating frequency to decrease. Also, the decreased $\overline{v}$ would reduce current and voltage generated by LG, which reduces the power output. The increased piston rod diameter could reduce the contact area between the air in cylinder B and the piston. For cylinder B, the resistance provided by air to piston during the exhaust stage would decrease, so that the acceleration of piston assembly moving from TDC to BDC increases, and BDC moves away from 0 point. Meanwhile, decreased contact area could lead the power which is provided by cylinder B to piston during the intake and expansion stage to decrease. The acceleration of piston assembly moving from BDC to TDC would decrease and v_{2max} would decrease. Both TDC and BDC move away from 0 point, and the interaction causes stroke to increase firstly and then decrease but the change is small. As TDC moves away from 0 point, the maximum pressure in cylinder A decreases, and the power provided to piston decreases, which makes v_{1max} and $\overline{v}$ decrease. With the stroke remaining almost unchanged, the operating frequency decreases. The decreased $\overline{v}$ would reduce the induced voltage and current, and thus the power output is reduced. The maximum value can reach up to 19.58 W.

(**a**) *S*, TDC, BDC.

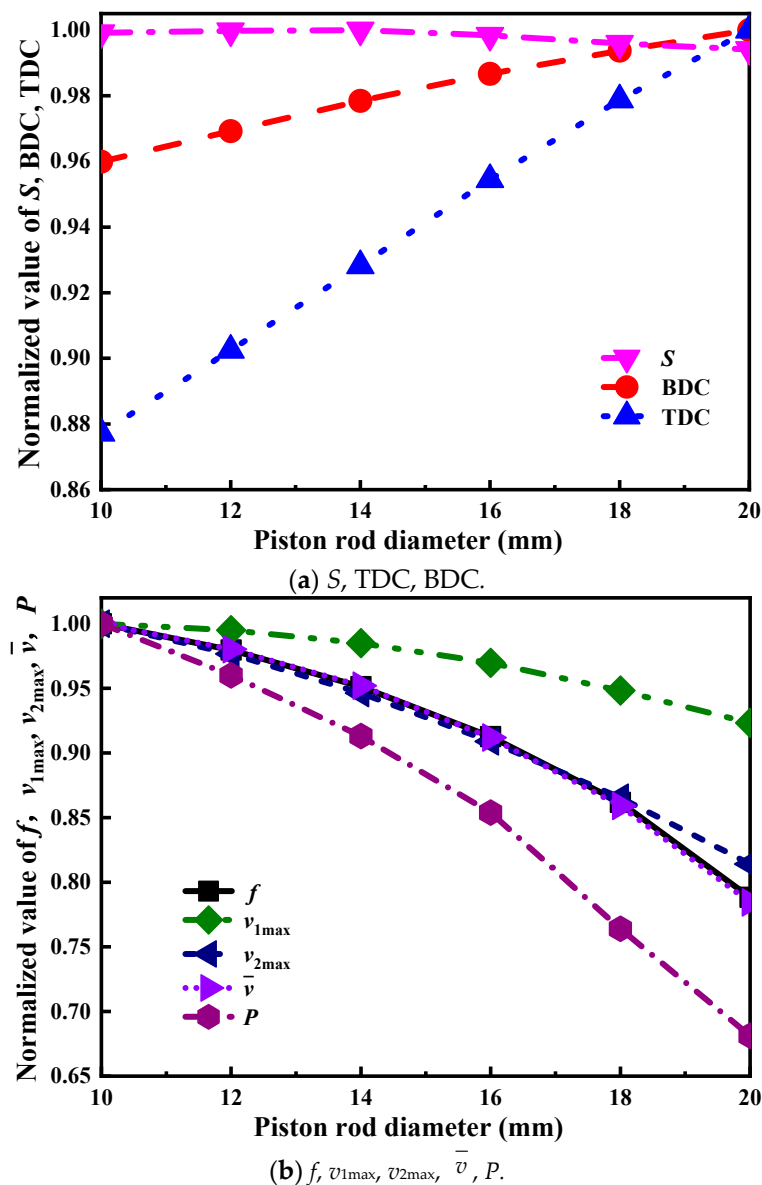(**b**) *f*, v_{1max}, v_{2max}, $\bar{v}$, *P*.

Figure 8. Variation of performance parameters with piston rod diameter.

3.1.5. Cylinder Diameter

Figure 9 shows the variation of normalized value of the performance parameters with cylinder diameter. TDC, BDC, and stroke all show a slight downward trend with the increase of cylinder diameter. The other performance parameters all increase with the increase in cylinder diameter. The increased cylinder diameter could increase the contact area between the air in the cylinder and the piston, and, thus, increase the force provided by the air to the piston. The increase in the force when piston assembly moves from BDC to TDC is greater than that from TDC to BDC, thus BDC and TDC move towards 0 point, and the interaction causes the stroke to reduce. The gas force in the cylinder on the piston increases, which increases the velocity of piston assembly. Through the interaction of decreased stroke and increased velocity, operating frequency decreases. In addition, the increased $\bar{v}$ enlarges the induced voltage and current generated by LG, leading power output to increase. The maximum value can reach up to 16.72 W.
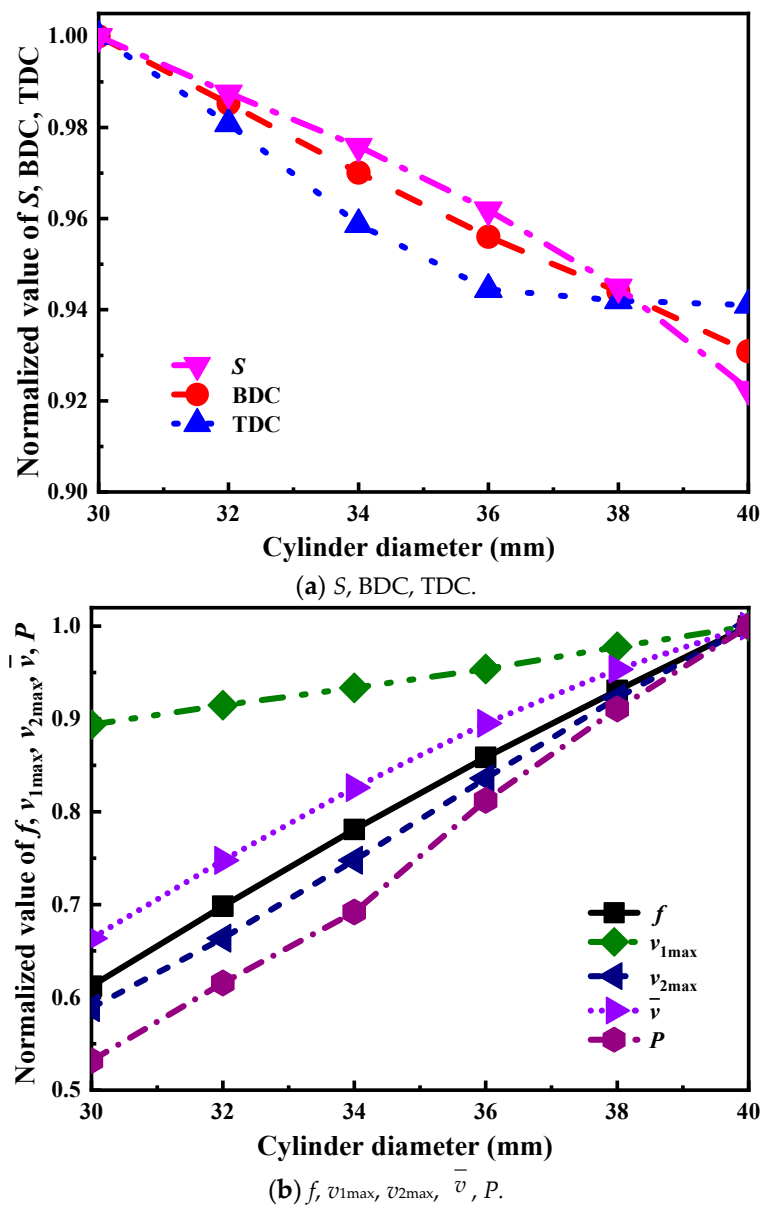
(a) *S*, BDC, TDC.

(b) f, v_{1max}, v_{2max}, $\bar{v}$, P.

Figure 9. Variation of performance parameters with cylinder diameter.

3.1.6. Diameter of Intake and Exhaust Pipes

Figure 10 shows the variation of normalized performance parameters with the diameter of intake and exhaust pipes. As can be seen in the figure, BDC, stroke, v_{1max}, and power output all show an upward trend with the increase of diameter of intake and exhaust pipes. Operating frequency, v_{2max}, and $\bar{v}$ all first increase and then decrease. However, TDC shows a trend of first decreasing and then increasing. The change in diameter of intake and exhaust pipes has a great influence on power output and v_{1max}. The influence of pipe diameter changes on FPE is mainly in the intake and exhaust stages. The change in pipe diameter directly affects the mass of intake and exhaust, which affects the force exerted on piston as well as the velocity and power output of piston assembly. The maximum value can reach up to 0.8 m/s and 18.98 W, respectively.
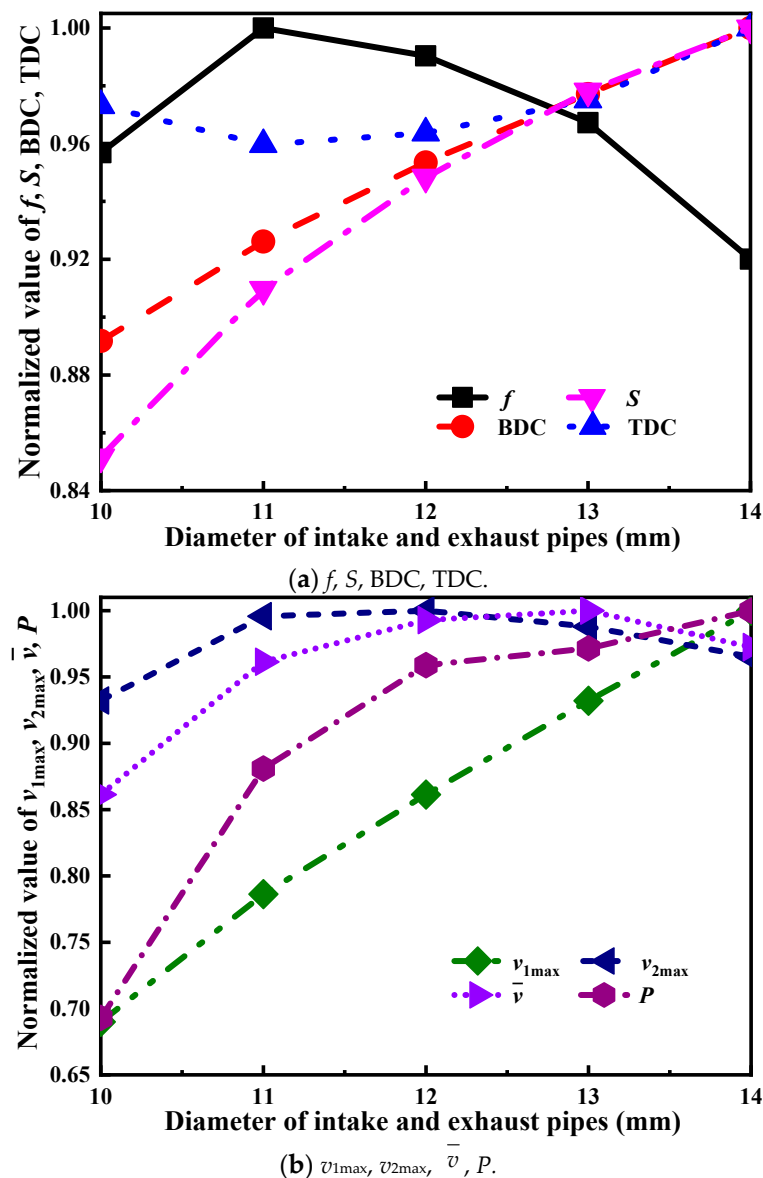
(**a**) f, S, BDC, TDC.

(**b**) v_{1max}, v_{2max}, $\bar{v}$, P.

Figure 10. Variation of performance parameters with diameter of intake and exhaust pipes.

3.2. Operating Parameters

3.2.1. Intake Beginning Position A

Figure 11 shows the variation of normalized performance parameters with intake beginning position A. As intake beginning position A moves away from 0 point, operating frequency, TDC, and BDC increase; stroke and v_{1max} decrease; and v_{2max}, $\bar{v}$ and power output first increase and then decrease. The trend of $\bar{v}$ is consistent with v_{2max} but different from v_{1max}, hence $\bar{v}$ is more affected by v_2 than by v_1 when intake beginning position A changes. When intake beginning position A is far from 0 point, the distance between the two intake beginning positions will be shortened, and TDC and BDC move away from 0 point, which leads the stroke to decrease. The moving of TDC and BDC also affects the cylinder volume during the intake stage, which causes the change of in–cylinder pressure and the velocity of piston assembly. The interaction of the changes in stroke and $\bar{v}$ increases the operating frequency. The interaction of velocity and operating frequency makes the power output increase first and then decrease. The maximum value can reach up to 18.54 W.
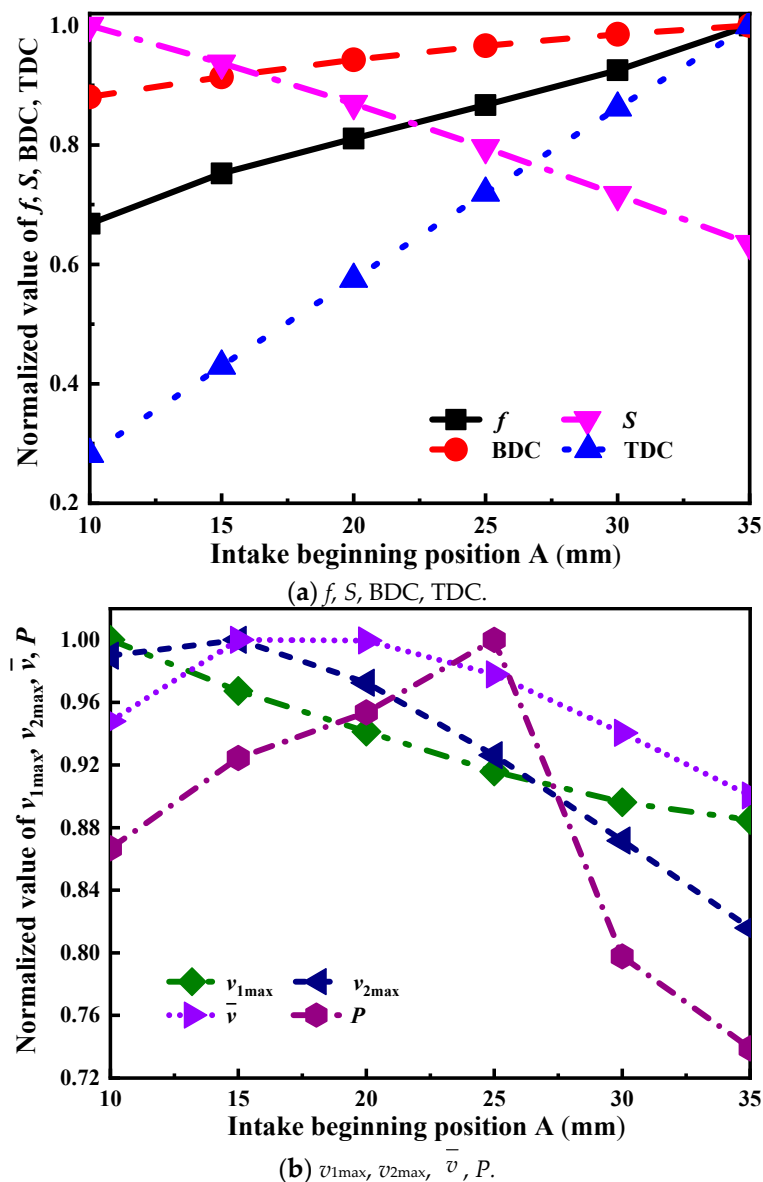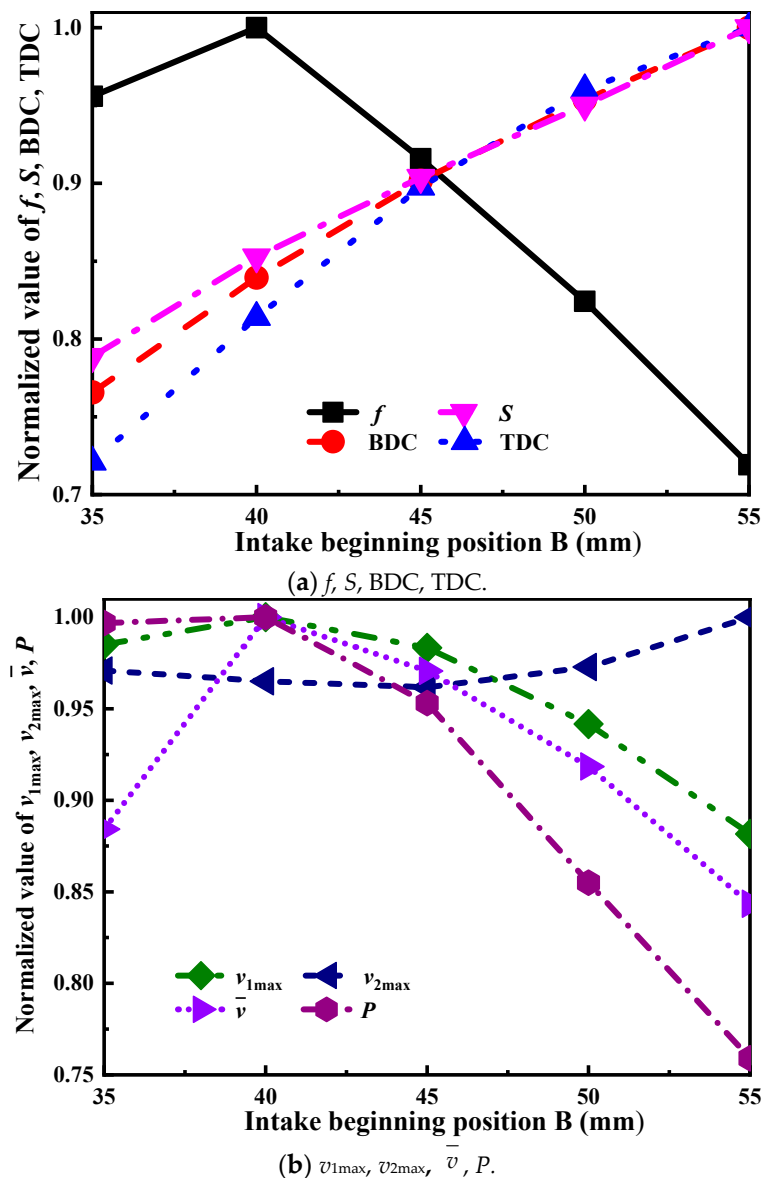
(**a**) *f*, *S*, BDC, TDC.

(**b**) v_{1max}, v_{2max}, $\overline{v}$, *P*.

Figure 11. Variation of performance parameters with intake beginning position A.

3.2.2. Intake Beginning Position B

Figure 12 shows the variation of normalized performance parameters with intake beginning position B. As intake beginning position B moves away from 0 point, operating frequency, power output, v_{1max}, and $\overline{v}$ all increase first and then decrease; TDC, BDC and stroke all increase; and v_{2max} first decreases and then increases. When intake beginning position B is far from 0 point, the distance between the two intake beginning positions increases, and both TDC and BDC move away from 0 point, which leads the stroke to increase. The moving of TDC and BDC also affects the cylinder volume during intake stage, which causes the change of in–cylinder pressure and the velocity of piston assembly. The interaction of the changes in stroke and $\overline{v}$ leads the operating frequency to increase first and then decrease. The interaction of velocity and operating frequency makes the power output increase first and then decrease. The maximum value can reach up to 18.76 W.

(**a**) f, S, BDC, TDC.

(**b**) v_{1max}, v_{2max}, $\bar{v}$, P.

Figure 12. Variation of performance parameters with intake beginning position B.

3.2.3. Intake Time

Figure 13 shows the variation of normalized performance parameters with intake time. It can be seen that operating frequency increases first and then decreases with intake time. BDC, power output, stroke, v_{1max}, v_{2max}, and $\bar{v}$ all tend to increase with intake time. The increased intake time could increase the in–cylinder pressure and the power provided by the air in cylinder, which leads to increase in the velocity of piston assembly and power output. The maximum value can reach up to 0.8 m/s and 26.68 W, respectively. Then the increase in velocity of piston assembly could cause the frictional resistance and electromagnetic resistance to increase. Under the interaction of impetus and resistance, TDC moves closer to 0 point, BDC moves away from 0 point, and the stroke increases. The interaction of the changes in stroke and velocity makes operating frequency increase first and then decrease.
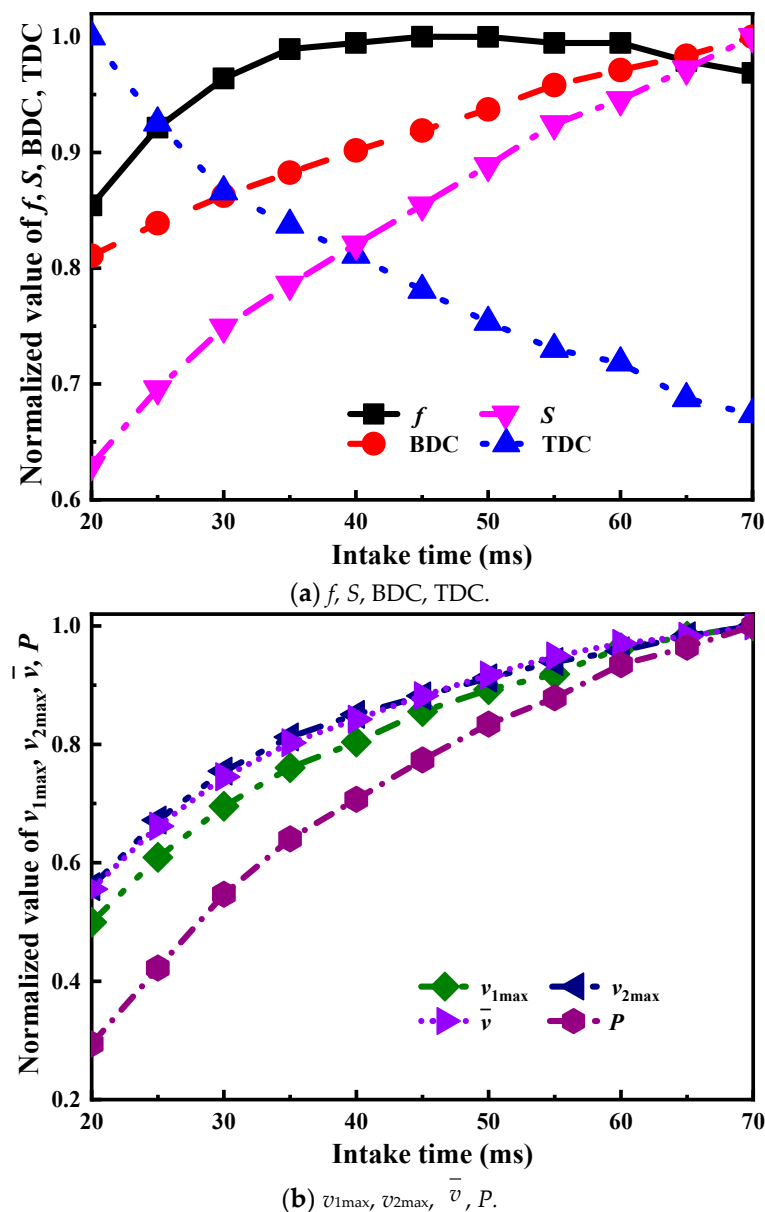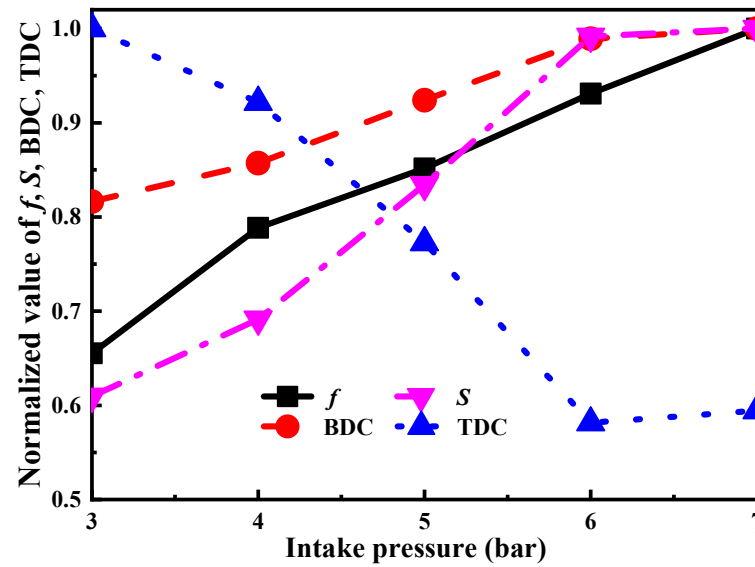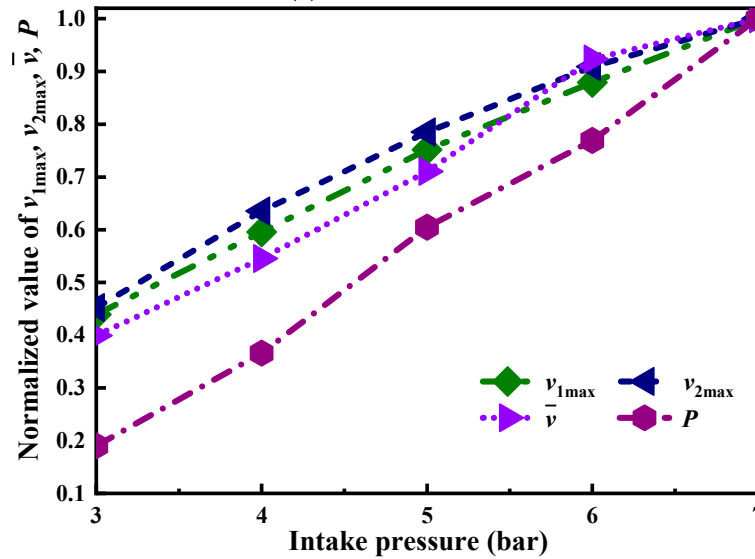
(a) *f*, *S*, BDC, TDC.

(b) v_{1max}, v_{2max}, $\bar{v}$, *P*.

Figure 13. Variation of performance parameters with intake time.

3.2.4. Intake Pressure

Figure 14 shows the variation of normalized performance parameters with intake pressure. With the increase of intake pressure, TDC first decreases and then increases, while all other parameters show an upward trend. Among them, the increase of the intake pressure from p_{in} = 6 bar to p_{in} = 7 bar has very little influence on TDC, BDC and stroke, where the change range of the normalized value is within 0.01. The increased intake pressure would make more compressed air flow into the cylinder, enhance the power exerted on piston, and increase the velocity of piston assembly, resulting in the increase of induced current and voltage, as well as the power output. The maximum value of the power output can reach up to 46.71 W. The increased velocity also leads to an increase in the frictional resistance and electromagnetic resistance. Under the interaction of impetus and resistance, TDC moves closer to 0 point, BDC moves away from 0 point, and the stroke increases. The increase in stroke is smaller than that in velocity, which increases the operating frequency.

(**a**) f, S, BDC, TDC.

(**b**) v_{1max}, v_{2max}, $\bar{v}$, P.

Figure 14. Variation of performance parameters with intake pressure.

3.2.5. External Load

Figure 15 shows the variation of normalized performance parameters with external load. With the increase of external load, TDC first decreases and then increases, power output first increases and then decreases, and other parameters show an upward trend. It can be seen that the external load has a greater influence on power output. The increased external load would reduce the electromagnetic coefficient, thus, the electromagnetic resistance would decrease, which increases the acceleration of piston assembly, stroke, and velocity. The increased external load could also reduce the induced current. Under the interaction of external load and the current, the power output first increases and then decreases. The maximum value can reach up to 17.08 W.
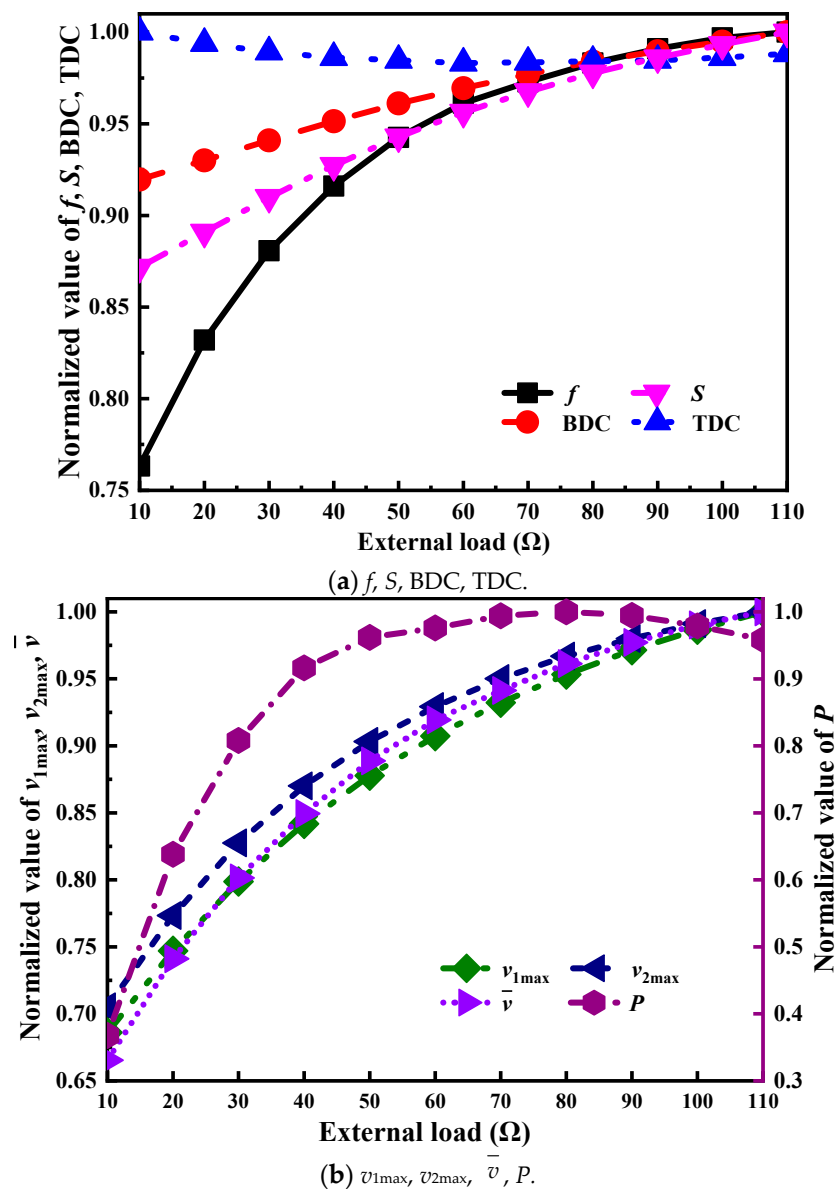
(**a**) *f*, *S*, BDC, TDC.

(**b**) v_{1max}, v_{2max}, $\bar{v}$, *P*.

Figure 15. Variation of performance parameters with external load.

3.3. Sensitivity Analysis

From the value of power output, it can be seen that the power output of FPE-LG is acceptable compared with other positive displacement expanders [47]. In addition, from the above trend, there are many factors affecting the performance of FPE-LG, so it is necessary to analyze its sensitivity from two aspects, that is, design and operating parameters.

3.3.1. Design Parameters

Figure 16 shows the influence of various design parameters on the power output. The abscissa represents the normalized value of design parameters, and the ordinate represents the normalized value of the power output. In order to better analyze the sensitivity of power output to design parameters, we mainly focused on the overlapping part in Figure 15. The order of power output sensitivity to design parameters from largest to smallest is cylinder diameter, back EMF constant, diameter of intake and exhaust pipes, piston rod diameter, frictional coefficient, and piston assembly mass. The power output is most sensitive to cylinder diameter, and increases with cylinder diameter. From an overall view, power output increases with increase of back EMF constant, cylinder diameter, and diameter of intake and exhaust pipes. In future structural design, it can be considered to increase the

values of these parameters to obtain higher power output. Power output decreases with the increase of piston rod diameter and frictional coefficient, so a smaller piston rod diameter and frictional coefficient can generate higher power output. For piston assembly mass, there is an optimal value to maximize power output.
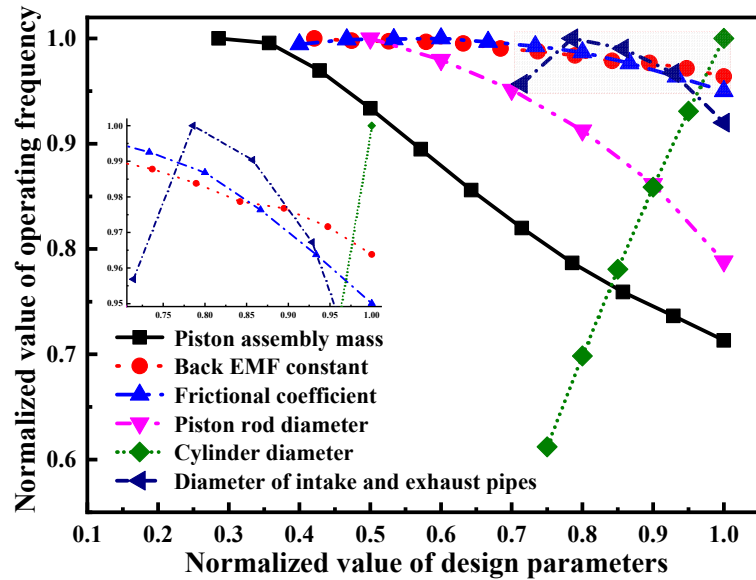

Figure 16. Influence of design parameters on power output.

Figure 17 shows the influence of various design parameters on the operating frequency. The abscissa represents the normalized value of the design parameters, and the ordinate represents the normalized value of the operating frequency. In the overlapping part, the sensitivity of the operating frequency in descending order is: cylinder diameter, piston rod diameter, piston assembly mass, diameter of intake and exhaust pipes, frictional coefficient, and back EMF constant. The operating frequency is most sensitive to cylinder diameter and increases with cylinder diameter, so a larger cylinder diameter can produce a higher operating frequency. Besides, operating frequency decreases with the increase of piston assembly mass, back EMF constant, and piston rod diameter. In future structural design, it can be considered to reduce the values of these parameters to obtain a higher operating frequency.
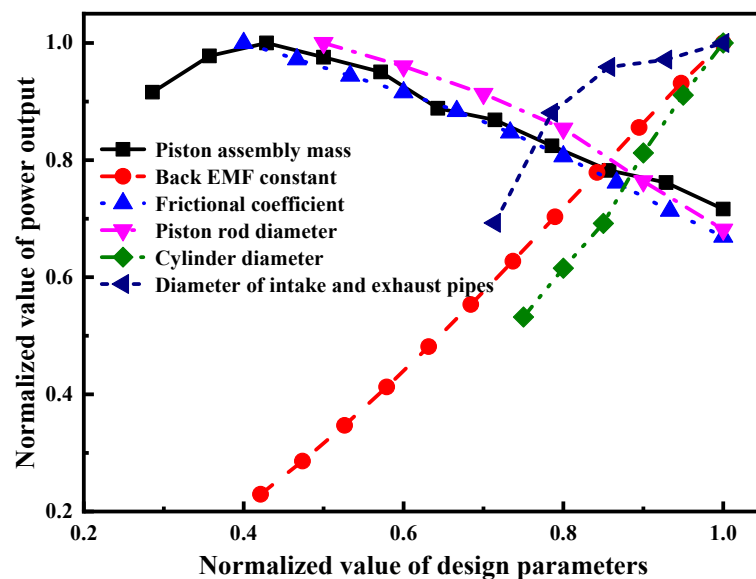

Figure 17. Influence of design parameters on operating frequency.

3.3.2. Operating Parameters

Figure 18 shows the influence of various operating parameters on the power output. The abscissa represents the normalized value of the operating parameters, and the ordinate represents the normalized value of the power output. In the overlapping part, the sensitivity of the power output to operating parameters from largest to smallest is: intake pressure, intake beginning position A, intake beginning position B, intake time, and external load. The power output is most sensitive to intake pressure and increases with it. The power output also increases with the increase of intake pressure and intake time. In future operation strategy, it can be considered to increase the value of these parameters to increase the power output. While for external load, intake beginning position A and B, there is an optimal value to maximize the power output.
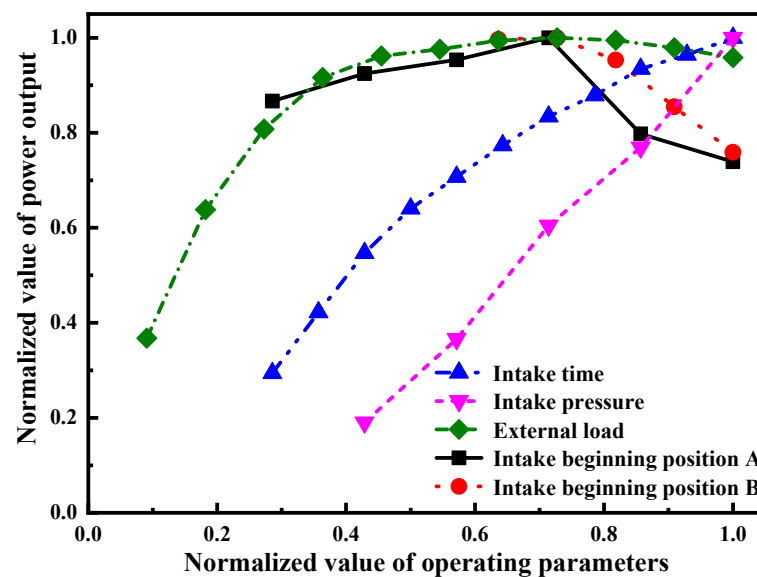

Figure 18. Influence of operating parameters on power output.

Figure 19 shows the influence of various operating parameters on operating frequency. The abscissa represents the normalized value of the operating parameters, and the ordinate represents the normalized value of the operating frequency. The order of operating frequency sensitivity in the overlapping part from largest to the smallest is intake beginning position B, intake pressure, intake beginning position A, intake time, and external load. Operating frequency increases with the increase of intake beginning position A, intake pressure, and external load. In future operation strategy, it can be considered to increase the values of these parameters to obtain a higher operating frequency.
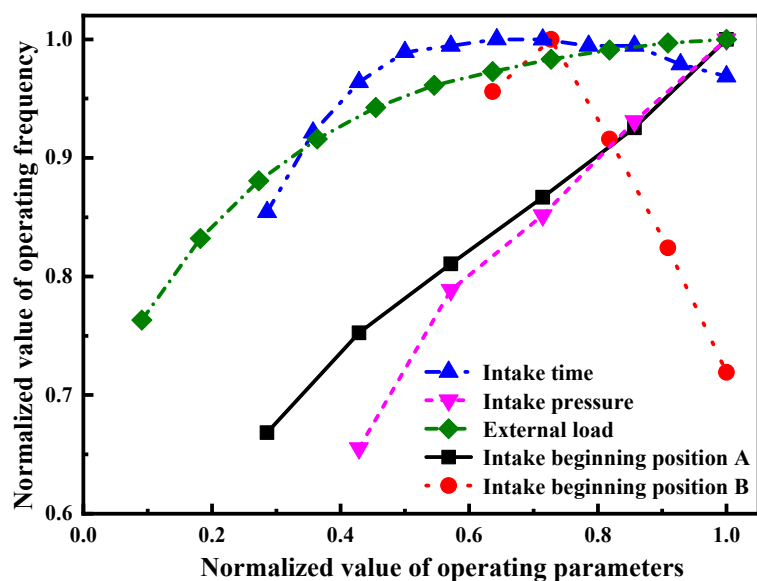
Figure 19. Influence of operating parameters on operating frequency.

4. Conclusions

Based on single–piston FPE–LG test rig, this paper builds a simulation model with MATLAB/simulink software. The validity and accuracy of the model are verified by the comparison and error analysis between the simulation results and experimental data. The influence mechanism of the design and operating parameters on FPE-LG performance is explored. By performing parameters normalization and sensitivity analysis, the sensitivity of design and operating parameters to power output and operating frequency is discussed. This research puts forward a new view of the structural design and operation strategy of single–piston FPE–LG, and lays the foundation for research on single–piston FPE–LG. The main conclusions are as follows:

(1) Among the involved design parameters, most parameters mainly affect the force exerted on the piston during operation, and the diameter of intake and exhaust pipes affects the mass of intake and exhaust. With the change of design parameters, the change range of power output is the largest among all performance parameters; when back EMF constant changes, the change range of power output is 80% of the maximum value.

(2) Among the involved operating parameters, intake beginning position A and B, intake time, and intake pressure mainly affect intake air mass; and external load affects the electromagnetic coefficient. With the increase in intake pressure and intake time, power output increases and the change range is up to 80% of the maximum value.

(3) Power output is most sensitive to cylinder diameter in design parameters and to intake pressure in operating parameters, and increases with the two parameters. Operating frequency is most sensitive to the cylinder diameter in the design parameters and increases with it. Operating frequency is most sensitive to the intake beginning position B in operating parameters, and first increases and then decreases with it. When intake beginning position B sites about 40 mm from 0 point, the operating frequency is the maximum.

Presently, the FPE-LG test rig has the limitation of small size and large vibration of the free piston. However, the advantages are also obvious, such as simple mechanical structure, low friction loss, and operational flexibility without crank linkage. Meanwhile, its control method has the advantages of simple and strong operability.

In the future, we will build the models of the ORC system and efficiency calculation, improve the current model with them, and study the ORC waste heat recovery system with an optimized FPE-LG in a more suitable operation strategy to improve its energy recovery efficiency as much as possible.

Nomenclature

A	contact area between air and piston in cylinder (m^2)
C	capacitance (F)
C_f	friction coefficient (N/(m·s^{-1}))
f	operating frequency (Hz)
E	induced voltage (V)
F_A, F_B	gas force exerted by the air in cylinder A, B (N)
F_e	electromagnetic resistance (N)
F_f	friction resistance (N)
I	induced current (A)
k	adiabatic coefficient
K_v	back EMF constant (V/(m·s^{-1}))
L	inductance (H)
m	piston assembly mass (kg)
p	in–cylinder pressure (bar)
p_e	intake or exhaust pressure (bar)
P	power output (W)
R	ideal gas constant (J/(mol·K))
R_e	external load (Ω)
R_S	internal resistance of LG (Ω)
s	displacement (m)
S	stroke (mm)
t	time (s)
T	temperature (K)
v	velocity of piston assembly (m/s)
$\bar{v}$	mean velocity of piston assembly (m/s)
Acronyms	
FPE	free piston expander
LG	linear generator
SACS	signal acquisition and control system
TDC	top dead center
BDC	bottom dead center
EMF	electromotive force
Greek letters	
μ_e	flow coefficient
Subscript	
1	from TDC to BDC
2	from BDC to TDC
max	maximum value

References

1.　Sansaniwal, S.K.; Sharma, V.; Mathur, J. Energy and exergy analyses of various typical solar energy applications: A comprehensive review. *Renew. Sustain. Energy Rev.* **2018**, *82*, 1576–1601. [CrossRef]
2.　Sahu, B.K. Wind energy developments and policies in China: A short review. *Renew. Sustain. Energy Rev.* **2018**, *81*, 1393–1405. [CrossRef]
3.　Xu, Y.H.; Zhang, H.G.; Yang, F.B.; Tong, L.; Yang, Y.F.; Yan, D.; Wang, C.Y.; Ren, J.; Wu, Y.T. Experimental study on small power generation energy storage device based on pneumatic motor and compressed air. *Energy Convers. Manag.* **2021**, *234*, 113949. [CrossRef]
4.　Wang, B.Z.; Yu, X.L.; Xu, H.M.; Wu, Q.; Wang, L.; Huang, R.; Li, Z.; Zhou, Q. Scenario analysis, management, and optimization of a new Vehicle-to-Micro-Grid (V2μG) network based on off-grid renewable building energy systems. *Appl. Energy* **2022**, *325*, 119873. [CrossRef]
5.　Huo, W.W.; Li, W.E.; Zhang, Z.H.; Sun, C.; Zhou, F.K.; Gong, G.Q. Performance prediction of proton-exchange membrane fuel cell based on convolutional neural network and random forest feature selection. *Energy Convers. Manag.* **2021**, *243*, 114367. [CrossRef]
6.　Guo, C.D.; Feng, H.H.; Jia, B.R.; Zuo, Z.X.; Guo, Y.Y.; Roskilly, T. Research on the operation characteristics of a free–piston linear generator: Numerical model and experimental results. *Energy Convers. Manag.* **2017**, *131*, 32–43. [CrossRef]
7.　Ping, X.; Yang, F.B.; Zhang, H.G.; Xing, C.D.; Zhang, W.J.; Wang, Y.; Yao, B.F. Dynamic response assessment and multi-objective optimization of organic Rankine cycle (ORC) under vehicle driving cycle conditions. *Energy* **2023**, *263*, 125551. [CrossRef]
8.　Yang, F.B.; Cho, H.J.; Zhang, H.G.; Zhang, J. Thermoeconomic multi–objective optimization of a dual loop organic Rankine cycle (ORC) for CNG engine waste heat recovery. *Appl. Energy* **2017**, *205*, 1100–1118. [CrossRef]
9.　Wu, L.M.; Feng, H.H.; Zhang, Z.W.; Jia, B.R.; Wang, J.Y.; Yang, F.Y.; Lei, Q.M. Experimental analysis on the operation process of opposed–piston free piston engine generator. *Fuel* **2022**, *325*, 124722. [CrossRef]
10.　Yang, F.B.; Zhang, H.G.; Bei, C.; Song, S.S.; Wang, E.H. Parametric optimization and performance analysis of ORC (organic Rankine cycle) for diesel engine waste heat recovery with a fin–and–tube evaporator. *Energy* **2015**, *91*, 128–141. [CrossRef]
11.　Ping, X.; Yang, F.B.; Zhang, H.G.; Xing, C.D.; Yu, M.Z.; Wang, Y. Investigation and multi-objective optimization of vehicle engine-organic Rankine cycle (ORC) combined system in different driving conditions. *Energy* **2023**, *263*, 125672. [CrossRef]
12.　Bahadori, M.N. Solar water pumping. *Sol. Energy* **1978**, *21*, 307–316. [CrossRef]
13.　Lemort, V.; Quoilin, S.; Cuevas, C.; Lebrun, J. Testing and modeling a scroll expander integrated into an Organic Rankine Cycle. *Appl. Therm. Eng.* **2009**, *29*, 3094–3102. [CrossRef]
14.　Badr, O.; O'Callaghan, P.W.; Hussein, M.; Probert, S.D. Multi-vane expanders as prime movers for low-grade energy organic Rankine-cycle engines. *Appl. Energy* **1984**, *16*, 129–146. [CrossRef]
15.　Tchanche, B.F.; Quoilin, S.; Declaye, S.; Papadakis, G.; Lemort, V. Economic feasibility study of a small scale organic rankine cycle system in waste heat recovery application. *Eng. Syst. Des. Anal.* **2010**, *49156*, 249–256.
16.　Ziviani, D.; James, N.A.; Accorsi, F.A.; Braun, J.E.; Groll, E.A. Experimental and numerical analyses of a 5 kWe oil-free open-drive scroll expander for small-scale organic Rankine cycle (ORC) applications. *Appl. Energy* **2018**, *230*, 1140–1156. [CrossRef]
17.　Tarique, M.A.; Dincer, I.; Zamfirescu, C. Experimental investigation of a scroll expander for an organic Rankine cycle. *Int. J. Energy Res.* **2014**, *38*, 1825–1834. [CrossRef]
18.　Zhang, Y.Q.; Wu, Y.T.; Xia, G.D.; Ma, C.F.; Ji, W.N.; Liu, S.W.; Yang, K.; Yang, F.B. Development and experimental study on organic Rankine cycle system with single–screw expander for waste heat recovery from exhaust of diesel engine. *Energy* **2014**, *77*, 499–508. [CrossRef]
19.　Yang, K.; Zhang, H.; Song, S.; Zhang, J.; Wu, Y.T.; Zhang, Y.Q.; Wang, H.J.; Chang, Y.; Bei, C. Performance analysis of the vehicle diesel engine-ORC combined system based on a screw expander. *Energies* **2014**, *7*, 3400–3419. [CrossRef]
20.　Fatigati, F.; Di Bartolomeo, M.; Cipollone, R. Dual intake rotary vane expander technology: Experimental and theoretical assessment. *Energy Convers. Manag.* **2019**, *186*, 156–167. [CrossRef]
21.　Fatigati, F.; Di Giovine, G.; Cipollone, R. Feasibility Assessment of a Dual Intake-Port Scroll Expander Operating in an ORC-Based Power Unit. *Energies* **2022**, *15*, 770. [CrossRef]
22.　Oudkerk, J.F.; Lemort, V. Detailed Experimental and Model-Based Analysis of a Swash-Plate Piston Expander for ORC Application. *Front. Energy Res.* **2020**, *8*, 107. [CrossRef]
23.　Zheng, N.; Zhao, L.; Wang, X.D.; Tan, Y.T. Experimental verification of a rolling–piston expander that applied for low–temperature organic Rankine cycle. *Appl. Energy* **2013**, *112*, 1265–1274. [CrossRef]
24.　Li, G.S.; Zhang, H.G.; Yang, F.B.; Song, S.S.; Chang, Y.; Yu, F.; Wang, J.F.; Yao, B.F. Preliminary development of a free piston expander–linear generator for small–scale organic Rankine cycle (ORC) waste heat recovery system. *Energies* **2016**, *9*, 300. [CrossRef]
25.　Pescara, R.P. Motor Compressor Apparatus. U.S. Patent 1057641, 31 January 1928.
26.　Zhang, B.; Peng, X.; He, Z.; Xing, Z.; Shu, P. Development of a double acting free piston expander for power recovery in trans critical CO_2 cycle. *Appl. Therm. Eng.* **2007**, *27*, 1629–1636. [CrossRef]
27.　Weiss, L.W. Study of a mems–based free piston expander for energy sustainability. *J. Mech. Des.* **2010**, *132*, 091002. [CrossRef]
28.　Preetham, B.S.; Weiss, L. Investigations of a new free piston expander engine cycle. *Energy* **2016**, *106*, 535–545. [CrossRef]
29.　Champagne, C.; Weiss, L. Performance analysis of a miniature free piston expander for waste heat energy harvesting. *Energy Convers. Manag.* **2013**, *76*, 883–892. [CrossRef]

30. Burugupally, S.P.; Weiss, L. Design and performance of a miniature free piston expander. *Energy* **2019**, *170*, 611–618. [CrossRef]

31. Hou, X.C.; Zhang, H.G.; Yu, F.; Liu, H.D.; Yang, F.B.; Xu, Y.H.; Tian, Y.M.; Li, G.S. Free piston expander–linear generator used for organic Rankine cycle waste heat recovery system. *Appl. Energy* **2017**, *208*, 1297–1307. [CrossRef]

32. Hou, X.C.; Zhang, H.G.; Zhao, T.L.; Xu, Y.H.; Tian, Y.M.; Li, J.; Zhang, M.R.; Wu, Y.T. A comparison study and performance analysis of free piston expander–linear generator for organic Rankine cycle system. *Energy* **2019**, *167*, 136–143. [CrossRef]

33. Hou, X.C.; Zhang, H.G.; Xu, Y.H.; Tian, Y.M.; Zhao, T.L.; Li, J.; Yu, F. Performance investigation of a free piston expander–linear generator for small scale organic Rankine cycle. *Appl. Therm. Eng.* **2018**, *144*, 209–218. [CrossRef]

34. Tian, Y.M.; Zhang, H.G.; Li, G.S.; Hou, X.C.; Yu, F.; Yang, F.B.; Yang, Y.X.; Liu, Y. Experimental study on free piston linear generator (FPLG) used for waste heat recovery of vehicle engine. *Appl. Therm. Eng.* **2017**, *127*, 184–193. [CrossRef]

35. Ismael, M.A.; Aziz, A.R.A.; Zainal, E.Z.; Mohammed, S.E.; Ayandotun, W.B.; Baharom, M.B.; Sallehudin, M.S.; Syakirin, M.R.; Anwerudin, A.R.T.; Masri, M.M. Investigation on free–piston motion and power generation of a dual–piston air–driven expander linear generator. *Energy Rep.* **2021**, *7*, 2388–2397. [CrossRef]

36. Ismael, M.A.; Aziz, A.R.A.; Zainal, E.Z.; Mohammed, S.E.; Baharom, M.B.; Anwerudin, A.R.T. Effect of generator configuration on the free–piston motion and power generation of air–driven expander system. *Alex. Eng. J.* **2022**, *61*, 3093–3104.

37. Wang, Y.D.; Chen, L.; Jia, B.R.; Roskilly, A.P. Experimental study of the operation characteristics of an air–driven free–piston linear expander. *Appl. Energy* **2017**, *195*, 93–99. [CrossRef]

38. Xu, Y.M.; Xue, X.F.; Wang, Y.D.; Ai, M.M. Performance characteristics of compressed air–driven free–piston linear generator (FPLG) system–A simulation study. *Appl. Therm. Eng.* **2019**, *160*, 114013. [CrossRef]

39. Peng, B.Y.; Tong, L.; Guo, C.D.; Huo, W.W. Experimental research and performance analysis of a free piston expander–linear generator coupled with a driving motor. *Energy Rep.* **2021**, *7*, 1349–1359. [CrossRef]

40. Li, J.; Yang, F.B.; Zhang, H.G.; Wu, Z.; Tian, Y.M.; Hou, X.C.; Xu, Y.H.; Ren, J. Comparative analysis of different valve timing control methods for single–piston free piston expander–linear generator via an orthogonal experimental design. *Energy* **2020**, *195*, 116966. [CrossRef]

41. Wu, Z.; Zhang, H.G.; Liu, Z.L.; Hou, X.C.; Li, J.; Yang, F.B.; Zhang, J. Experimental study on the performance of single–piston free–piston expander–linear generator. *Energy* **2021**, *221*, 119724. [CrossRef]

42. Wu, Z.; Zhang, H.G.; Liu, Z.L.; Tian, G.H.; Hou, X.C.; Yang, F.B. Force and energy analysis of single–piston free–piston expander–linear generator. *Energy* **2022**, *251*, 123926. [CrossRef]

43. Tian, C.L.; Feng, H.H.; Zuo, Z.X. Oscillation characteristic of single free piston engine generator. *Adv. Mater. Res.* **2012**, *383*, 1873–1878. [CrossRef]

44. Zhao, T.L.; Zhang, H.G.; Hou, X.C.; Xu, Y.H.; Li, J.; Shi, X.; Wu, Y.T. Modelling and validation of a free piston expander–linear generator for waste heat recovery system. *Appl. Therm. Eng.* **2019**, *163*, 114377. [CrossRef]

45. Xu, Y.H.; Tong, L.; Zhang, H.G.; Hou, X.C.; Yang, F.B.; Yu, F.; Yang, Y.X.; Liu, R.; Tian, Y.M.; Zhao, T.L. Experimental and simulation study of a free piston expander–linear generator for small–scale organic Rankine cycle. *Energy* **2018**, *161*, 776–791. [CrossRef]

46. Xiao, J.; Li, Q.F.; Huang, Z. Motion characteristic of a free piston linear engine. *Appl. Energy* **2010**, *87*, 1288–1294. [CrossRef]

47. Kolasiński, P. Application of the multi-vane expanders in ORC systems—A review on the experimental and modeling research activities. *Energies* **2019**, *12*, 2975. [CrossRef]